processes

MDPI

Article

Characterization on Structure and Fractal of Shale Nanopore: A Case Study of Fengcheng Formation in Hashan Area, Junggar Basin, China

Weizheng Gao [1], Xiangchun Chang [1,*], Pengfei Zhang [1], Zhongquan Liu [2], Zhiping Zeng [2], Yue Wang [1] and Tianchen Ge [1]

[1] College of Earth Science and Engineering, Shandong University of Science and Technology, Qingdao 266590, China
[2] Research Institute of Petroleum Exploration and Development, Shengli Oilfield Company, Sinopec, Dongying 257015, China
* Correspondence: xcchang@sdust.edu.cn

Abstract: The Lower Permian Fengcheng Formation in Halaalate Mountain in the Junggar Basin has enormous potential for shale oil, while few investigations on quantifying pore structure heterogeneity have been conducted. Thus, total organic carbon (TOC), X-ray diffraction (XRD), scanning electron microscopy (SEM), and low-temperature N_2 adsorption tests were conducted on the shales collected from the HSX1 well in the Hashan region to disclose the microscopic pore structure and its heterogeneity. Results show that the selected shales mainly consist of quartz, plagioclase, calcite, and clay minerals. The primary pore types are intergranular pores in quartz and carbonate and intragranular pores in clays, while organic matter (OM) pores are rare. Typical types of H2 and mixed H2-H3 were observed. Type H3 shale pore size distributions (PSD) are unimodal, with a peak at about 70 nm, while Type H2-H3 shales are bimodal, with peaks at about 70 nm and 3 nm, respectively. Type H3 shales have lower D_2 than Type H2-H3 shale, corresponding to weaker pore structure heterogeneity. Multifractal analyses indicate that macropores in Type H3 shales have stronger heterogeneity with large $D_{10}-D_0$ ranges, while minor $D_{-10}-D_0$ ranges mean weaker heterogeneity of micro- and mesopores, and so do Types H2-H3 shales. The higher the contents of plagioclase and clay minerals, the more heterogeneous the micro- and mesopores are; a larger content of quartz leads to more heterogeneous macropores. Specific surface area, micro-, and mesopores contents positively correlate to D_2, while average pore diameter and macropores are on the contrary, thus the higher the content of micro- and mesopores and the specific surface area, the lower the content of macropores and average pore diameter, the more complex the microscopic pore structure of shale. Micro- and mesopores control the heterogeneity of shale pore development with a great correlation of $D_{-10}-D_0$ and $D_{-10}-D_{10}$, and D_2 can effectively characterize the heterogeneity of a high porosity area with a strong correlation of D_2 and D_0-D_{10}.

Keywords: pore structure; fractal dimension; low-temperature nitrogen adsorption; shale oil; Halaalate mountain

Citation: Gao, W.; Chang, X.; Zhang, P.; Liu, Z.; Zeng, Z.; Wang, Y.; Ge, T. Characterization on Structure and Fractal of Shale Nanopore: A Case Study of Fengcheng Formation in Hashan Area, Junggar Basin, China. *Processes* **2023**, *11*, 677. https://doi.org/10.3390/pr11030677

Academic Editor: Qingbang Meng

Received: 1 February 2023
Revised: 20 February 2023
Accepted: 21 February 2023
Published: 23 February 2023

1. Introduction

With the deepening of unconventional oil and gas exploration in recent years, shale oil has become an increasingly important component of global energy. Commercially successful production of unconventional shale oil and gas in the United States has prompted China to learn and introduce shale oil development and extraction technologies and has increased its efforts to explore shale oil resources [1]. The shale oil resources of China are considerable, and the recoverable resource of medium–high maturity shale oil is enormous at present; continental shale oil has become the most potential oil resource in China and has a reasonable prospect for exploration and development [2].

Shale is a complex heterogeneous porous medium, shale oil has nanoscale pores and exists in shale formations, essentially without any migration mechanism; it represents mature organic shale oil, which is mainly filled in microscopic pores and fracture systems in adsorbed and free states [3,4]. Unconventional shale has a complex pore structure, high heterogeneity, and small nanopore size; the complexity and heterogeneity of its pore structure are the key factors to control the occurrence and flow of shale oil, which is difficult to characterize effectively by traditional methods [5]. Currently, the methods of pore structure characterization and fractal theory are mainly used to discuss the microscopic characteristics and heterogeneity of the pore system [6,7].

There are currently many methods used to study the microscopic pore structure of shale. Direct methods to analyze shale microscopic pore structure characteristics are X-ray computer scanning and scanning electron microscopy (SEM) [8–12]. These methods can obtain pore morphology and connectivity directly. Indirect methods such as N_2 and CO_2 adsorption, nuclear magnetic resonance, and high-pressure mercury injection can yield quantitative porosity, pore volume, specific surface area, pore size distribution, and other structural parameters [13–17]. There are also wave propagation and attributes, such as energy losses (scattering and intrinsic attenuation), that are methods of analyzing shale indirectly [18,19]. Shale pore type, shape, and quantitative heterogeneity affect the migration and storage of shale oil. The fractal theory can be effectively used to quantitatively evaluate pore structure complexity and heterogeneity. Previous research has shown that N_2 adsorption experiments combined with the FHH model have been widely applied to calculate the fractal dimension to characterize the heterogeneity of the pore structure; the single fractal characterizes the average property of the pore structure. However, the large number of nanopores present in the shale pore structures and the complexity of the structures make it difficult for the single-fractal models to describe all characteristics of shale pore structures. The multi-fractal divides the pore structure into several regions and studies the heterogeneity of pore structure separately and it has been proved that it can effectively describe the pore characteristics of shale [20–24].

The Junggar Basin is a large stacked oil-containing gas basin in western China, and the northwest part is one of the main oil and gas gathering areas in the basin [25]. The Lower Permian Fengcheng Formation is mainly a semi-closed residual marine environment of a rift basin with widely distributed and abundant hydrocarbon source rocks. It is an important reservoir of unconventional oil reservoirs. In recent years, exploration studies have found that the Permian Fengcheng Formation in the Hashan area is rich in oil and gas, indicating a broad prospect for shale oil development [26,27]. Previous studies mainly focused on the macroscopic research of the Fengcheng Formation in the Hashan area, such as sedimentary environment and sedimentary facies, reservoir development, tectonic fracture genesis, etc. Still, they ignored the heterogeneity of microscopic pore structure and pore size distribution of shale, and the shale pore system of the Fengcheng Formation is not fully understood [25,28–31].

Based on the above research, this study selected shale samples from well HSX1 of the Fengcheng Formation of the Permian System, studied the microscopic characteristics of the pore system through TOC, XRD, SEM, low-temperature N_2 adsorption experiments, and focused on studying the heterogeneity of pore structure and its influencing factors through fractal theory. Furthermore, pore structure analysis tests the adaptability of single fractal and multifractal in shale reservoirs. The results are relevant for providing insight into the pore distribution and its heterogeneity in oil-bearing shale in the Fengcheng Formation, Junggar Basin.

2. Geology Setting

The Hashan area is located in the northwest margin of the Junggar Basin in China, with an exploration area of up to 1000 km^2, which is an important area for continental accumulation and orogenic movement (Figure 1a,b) [26]. The structural belt of the Hashan area presents a banded distribution on the plane, high in the northeast and low in the

southwest, and the tectonic activities are frequent and the tectonic characteristics are quite complicated. There are six tectonic evolutions from Late Carboniferous to Cenozoic; the Late Permian to Triassic is the most intense period of tectonic activity in the Hashan area, at which time the main structure of Hashan was formed [32,33]. The rapid maturation of source rocks in the footwall of the nappe body in the Hashan area was affected by the strong thrust and nappe at the end of the Early Permian, Late Permian, and Triassic periods, then forming the Hashan region's oil and gas [34]. The Fengcheng Formation can be divided into three parts from bottom to top: the first member of the Fengcheng Formation mainly develops fine-grained mixed rocks, such as argillaceous dolomite and dolomite mudstone, while the bottom develops explosive facies volcanic rocks; the second member of the Fengcheng Formation is primarily composed of dolomite, argillaceous dolomite, and other mixed rocks, intercalated with thin explosive facies volcanic rocks; the third member is predominantly composed of sedimentary clastic rocks with fine lithology [27,28]. The shale oil reservoirs of the Fengcheng Formation are mainly restricted by sedimentary facies, diagenesis, and tectonic activities, in which the sedimentary facies developed a transgressive to regressive water model, and the shore-shallow lake and semi-deep lake sedimentary facies provided a large number of source rocks; evident dissolution considerably enhances reservoir character and provides space for shale oil occurrence; strong tectonic activity produced numerous micro-fractures and routes for the migration of oil and gas, forming a good shale oil reservoir, thus showing that the Fengcheng Formation shale has enormous potential for shale oil [35,36].

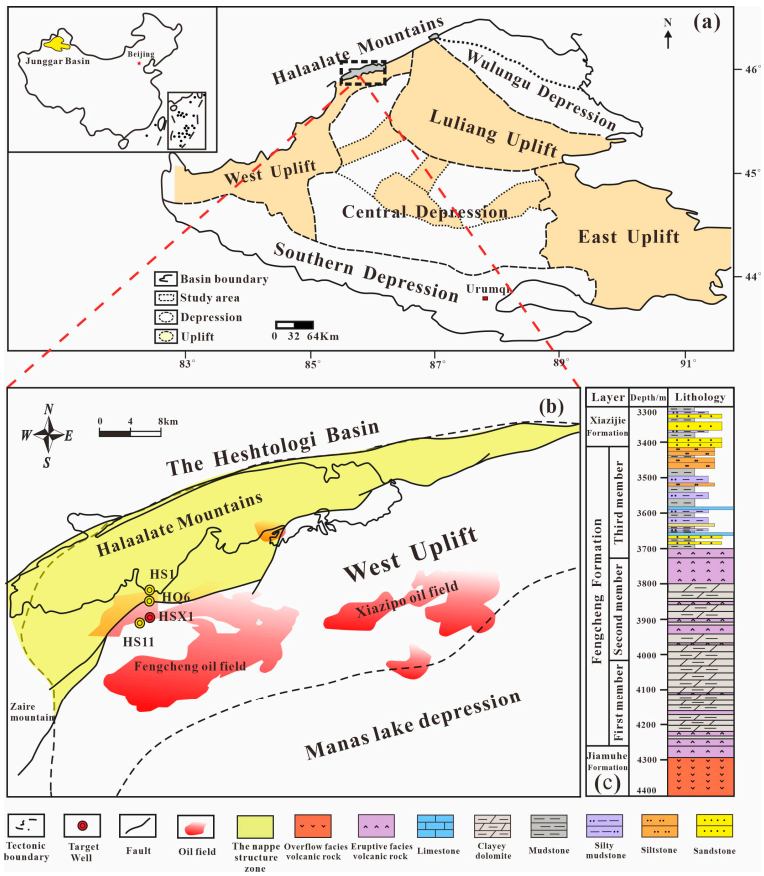

Figure 1. Regional tectonic location of Hashan area and the stratigraphic column of the Permian Fengcheng Formation: (**a**) Location of the Junggar Basin within China. (**b**) Tectonic location of Hashan area in northwestern margin of Junggar Basin. (**c**) lithostratigraphic column of Permian Fengcheng Formation of well HSX1.

3. Methods and Theories

3.1. Samples and Experiments

Seven shale samples were collected from well HSX1 of the Fengcheng Formation. A series of experiments were conducted, including total organic carbon (TOC), X-ray diffraction (XRD), scanning electron microscopy (SEM), and low-temperature N_2 adsorption (NGA).

The shale samples were crushed to 100 mesh and tested for TOC content using a LECO-CS-230 carbon/sulfur analyzer. The entire rock and clay mineral components of shale were analyzed by a D8 DISCOVER X-ray diffractometer. The instrument radiates with ka as a parameter and measures at a speed of 2(°) (2θ)/min in the range of 2.6–45° (2θ). The emission and scattering slits are 1°, the acceptance slit is 0.3 mm, and the sampling width is 0.02° (2θ). The test was carried out according to the standard SY/T 5163-2018 Method for X-ray diffraction analysis of clay minerals and common non-clay minerals in sedimentary rocks.

A Phenom Pro X desktop scanning electron microscope was used for imaging pore morphology. The samples were cut perpendicular to bedding first, then mounted on a short column, and polished of the surface. The surface was further polished by argon ion to obtain a flat surface. The resolution of SEM image is better than 6 nm, with an optical amplification of up to 350,000 times. And the backscattered images and energy spectrum scanning at appropriate points was also conducted.

The shale low-temperature N_2 adsorption experiment was performed using a Micromeritics ASAP 2460 specific surface area and porosity analyzer. Shale samples were first crushed to grain sizes of 40–60 mesh (0.18–0.25 mm), then residual oil in shale pores was removed using dichloromethane and acetone solution (3:1 in volume) for 7 days at a pressure of 0.2 MPa and temperature of 80 °C and dried at 110 °C for 24 h in a vacuum oven. Finally, N_2 adsorption–desorption isotherms at 77 K were obtained in the relative pressure (p/p_0) range of 0.01 to 0.993. In this study, the total pore volume (PV), specific surface area (SSA), and average pore diameter (d_a) were all obtained from the adsorption branch. According to the pore size of shale, the pore classification method of IUPAC was used in this paper: micropore (<2 nm), mesopore (2–50 nm), and macropore (>50 nm).

3.2. Fractal Dimension

Shale is a porous medium with a complicated microscopic pore structure and shale pores are dispersed throughout three-dimensional space. Thus, it is challenging to accurately characterize the complexity and variety of the shale micro-pore structure. By employing the adsorption theory, Pfeifer et al. [37] proved that the pores in rock reservoirs have fractal characteristics. According to Krohn [38], the pores in shale and sandstone show fractal characteristics. As a result, the fractal theory is applied to describe the heterogeneity of the microscopic pore structure of shale, which also offers a novel method for quantitatively assessing the pore structure complexity.

This study realized the fractal analysis of pores through the FHH (Frenkel–Halsey–Hill) model based on the adsorption branch [39–41]. The calculation of single fractal dimensions can be described as follows:

$$ln(\frac{V}{V_0}) = A[ln(ln(\frac{p_0}{p}))] + C \quad (1)$$

where P represents the equilibrium pressure and V represents the adsorbed gas volume at equilibrium pressure; V_0 is the volume of monolayer N_2 adsorption; P_0 denotes the saturated vapor pressure of nitrogen at 77 K; C is a constant and A is the slope. The slope A can be used to determine the single fractal dimension D.

$$D = A + 3 \quad (2)$$

The equation above has been frequently used [40–42].

The multifractal model is an extension of fractal theory, and the generalized fractal dimension *q*-*Dq* is a method to describe local multifractal characteristics. It needs to determine two parameters, the mass probability p_i (ε) and the generalized fractal dimension, D_q. The key step is to use the box-counting method to deal with the N_2 adsorption in different intervals as the research object to analyze the heterogeneity of pore distribution. The length L of the study interval is divided into 2^k boxes of the same size according to the dichotomy principle, and the size of ε is $L \times 2^{-k}$ (k = 0,1,2, . . .), and different box sizes ε are defined as p_i (ε). By employing this technique, the local distribution characteristics within the study object are quantitatively described [15,17]. The p_i (ε) can be quantified as:

$$p_i(\varepsilon) = \frac{N_i(\varepsilon)}{N_i} \tag{3}$$

where N_i (ε) represents the N_2 adsorption amount in the ith box, N_i is the total N_2 adsorption amount, p_i (ε) stands for the ith box's mass probability function, D_q can be expressed as:

$$D_q = \lim_{\varepsilon \to 0} \frac{1}{q-1} \frac{lg[\sum_{i=1}^{N(\varepsilon)} p_i^q(\varepsilon)]}{lg(\varepsilon)} \tag{4}$$

where q is the order of statistical moments, and the change of its data reflects the probability distribution characteristics of the research object. D_q represents the complexity of shale fractal structure at different local levels. The value of D_q represents the characteristics of the pore heterogeneity in the low-porosity region when $q < 0$, and the value of D_q stands for the nature of the pore heterogeneity in the high porosity region when $q > 0$. The D_q value with a step size of 2 is calculated according to the above formula and can draw the generalized dimensional spectrum through a series of data points of q and D_q.

$a \sim f(a)$ is another basic mathematical tool for describing the local characteristics of multifractality, called the multifractal spectrum. p_i (ε) can also be defined by an exponential function of the following form for each box of size ε as:

$$p_i(\varepsilon) \sim \varepsilon^{-a_i} \tag{5}$$

where a_i can reflect the local singular strength and represents the size of the region probability. Additionally, $N_a(\varepsilon)$ stands for the quantity of singular strength boxes between a and $a + da$, and it has the following relationship with ε:

$$N_a(\varepsilon) \sim \varepsilon^{-f(a)}, \varepsilon \to 0 \tag{6}$$

a and $f(a)$ can be determined using the CHHABRA and JENSEN methods [43], the formulas are as follows:

$$a(q) \infty \frac{\sum_{i=1}^{N(\varepsilon)} [u_i(q,\varepsilon) lg\varepsilon]}{lg\varepsilon} \tag{7}$$

$$f(a) \infty \frac{\sum_{i=1}^{N(\varepsilon)} [u_i(q,\varepsilon) lg u_i(q,\varepsilon)]}{lg\varepsilon} \tag{8}$$

$$u_i(q,\varepsilon) = \frac{{p_i}^q(\varepsilon)}{\sum_{i=1}^{N(\varepsilon)} {p_i}^q(\varepsilon)} \tag{9}$$

The partition function that is the denominator in Equation (9) for multifractals is written as:

$$x(q,\varepsilon) = \sum_{i=1}^{N(\varepsilon)} p_i{}^q(\varepsilon) \quad (10)$$

For a certain statistical moment order q, a mass exponential function is one that meets the conditional criterion $x(q,\varepsilon) \infty \varepsilon^{i(q)}$, if $i(q)$ and q are convex functions, it indicates that the research object has multifractal properties.

4. Results

4.1. Mineral Compositions of Shales

The results of XRD show that the minerals of the studied shales are mainly composed of quartz, calcite, clay minerals, and plagioclase (Table 1). Quartz contents range from 5.59% to 71.64%, with an average of 42.75%. Calcite content varies from 11.16% to 57.16%, with a mean of 23.01%. Clay minerals range from 7.93% to 19.56% (mean 15%), and the content of plagioclase is between 4.05% and 28.04% (mean 13.99%). In addition, shales also contain tiny amounts of pyrite and potassium feldspar. The studied shales are characterized by low clay and high brittle minerals, and the brittle minerals (quartz and feldspar) average 60.72%, with a maximum of 78.18% (Figure 2).

Table 1. Mineral compositions of shale samples.

Sample	Depth/m	Whole Rock Mineral/%					
		Quartz	Potash Feldspar	Plagioclase	Calcite	Pyrite	Clay
HSX1-1	3345.10	51.50	0.00	13.49	17.63	3.06	14.33
HSX1-2	3345.50	43.72	0.00	12.41	21.16	3.29	19.42
HSX1-4	3347.00	36.79	4.80	15.57	18.53	4.76	19.56
HSX1-6	3348.90	5.59	3.29	11.22	57.16	2.93	19.81
HSX1-7	3424.22	51.07	0.00	13.18	24.18	3.65	7.93
HSX1-8	3349.55	71.64	1.58	4.05	11.29	1.16	10.27
HSX1-12	3352.22	38.94	5.08	28.04	11.16	3.10	13.68

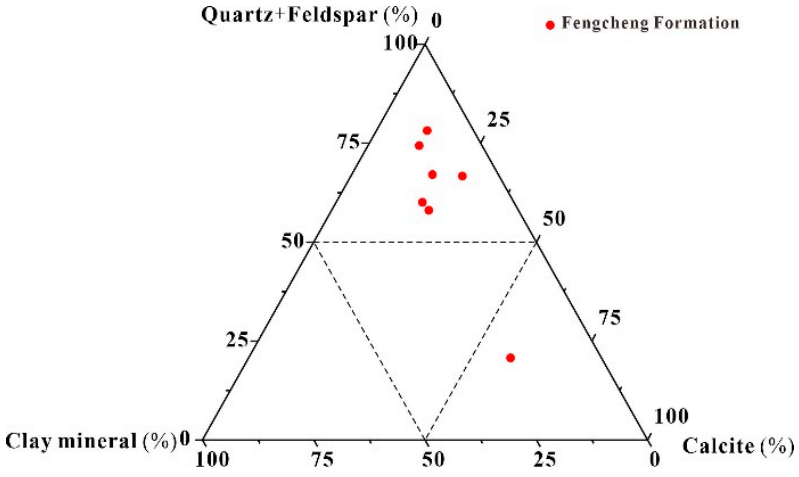

Figure 2. Shale sample mineralogical composition ternary diagram.

4.2. Shale Pore Types

The primary pore types of the selected shales are intergranular pores between quartz and carbonate and the intragranular pores in clay mineral aggregates. However, intergranular pores between feldspar are less developed, and organic matter (OM) pores are rare.

Therefore, inorganic pores constitute the main storage space for shale oil (Figure 3). The intergranular pores between quartz particles appear as irregular polygons and triangles, with significant variations in pore size (Figure 3a,b). The intergranular pores between calcite particles are characterized by irregular spherical and crescent shapes (Figure 3d,e). Additionally, intergranular pores related to feldspar show narrow shapes (Figure 3c). The pores within the clay mineral are developed in the flocculent aggregates with more complex pore shapes and vary greatly due to the serious deformation by compaction. However, these pores have poor connectivity with each other due to the small pore diameters (Figure 3f). Therefore, it can be concluded that the primary pore types are intergranular pores, such those associated with quartz and carbonate, which significantly increase reservoir space, while intragranular pores in clay minerals contribute less to reservoir space.

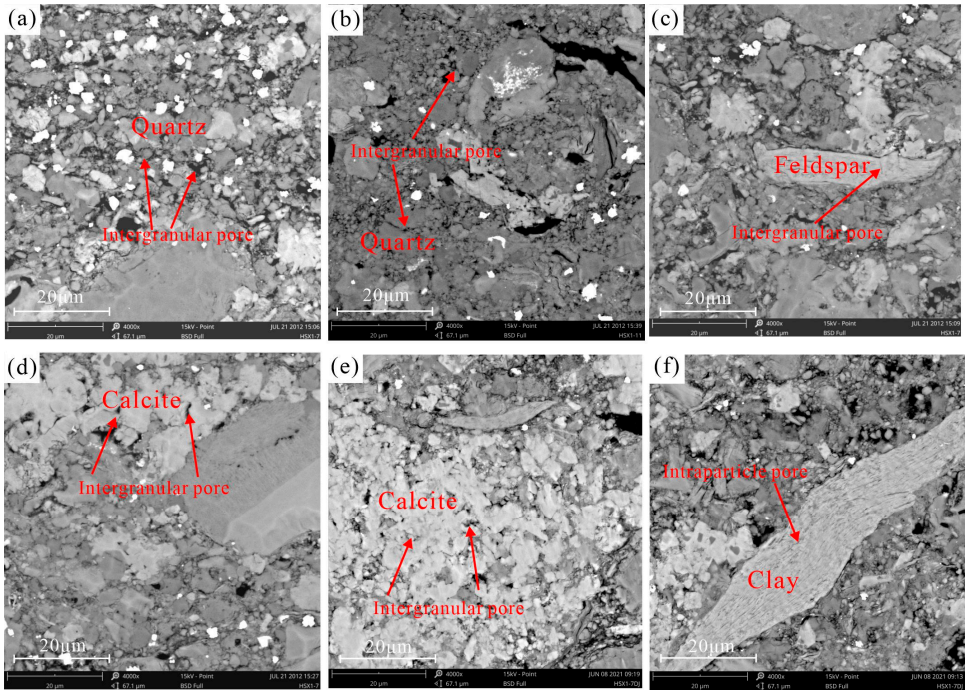

Figure 3. Types of shale reservoir space from Fengcheng Formation: (**a**,**b**) Interparticle pores at the edge of quartz. (**c**) Interparticle pores at the edge of feldspar. (**d**,**e**) The intergranular pores between calcite particles. (**f**) Intraparticle pores at the inside of clay minerals.

4.3. Micropore Structures of Shales

4.3.1. N_2 Adsorption—Desorption Isotherms

According to the latest classification recommended by IUPAC [44], the studied shales belong to the typical type IV isotherm. The N_2 gradually adsorbs on the pore surface, forming the adsorption branch. As the pressure decreases, the nitrogen gradually desorbs on the surface of the shale, forming the desorption branch. With the increase of the relative pressure, the nitrogen adsorption capacity gradually increased, and finally, all samples did not reach adsorption saturation. Additionally, when the relative pressure is less than 0.45, the adsorption and desorption curves almost overlap. However, the desorption curve is higher than the adsorption curve when the relative pressure is greater than 0.45, forming a hysteresis loop that can effectively indicate the predominant pore shapes in shale.

According to the shape of the hysteresis loop of N_2 adsorption–desorption isotherms, the seven shale samples examined can be classified as Types H3 and H2-H3. The adsorption–desorption isotherms of Type H3 shales show a slowly rising trend when the relative pressure is in the range of 0~0.5, and increase abruptly when the relative pressure is close to p_0, indicating a narrow hysteresis loop associated with the parallel plate pores (Figure 4b). For Type H2 shales, when the relative pressure is close to 0.5, the desorption branch has a

clear inflection point and forms a hysteresis loop, reflecting the ink bottle-shaped pores. However, for Type H2-H3 shales, the desorption branches are visibly convex and form hysteresis loops, implying that the ink bottle and slit pores occur concurrently (Figure 4a). Slit pores are relatively developed, which is similar to the study of Jiang. et al. [45].

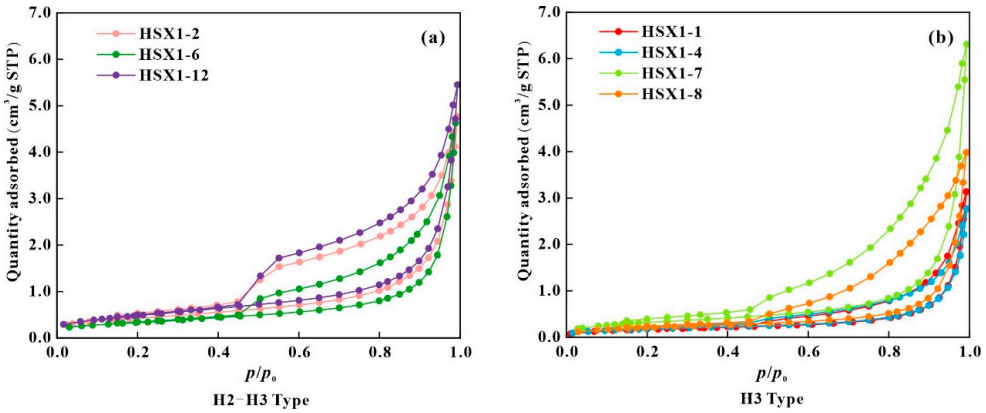

Figure 4. N_2 adsorption–desorption isotherms of shales from Fengcheng Formation: (**a**) Nitrogen adsorption-desorption isotherms of Type H2-H3 shales. (**b**) Nitrogen adsorption-desorption isotherms of Type H3 shales.

4.3.2. Microscopic Pore Structures

The SSA of the seven samples ranges from 0.5971 m^2/g to 1.7765 m^2/g, with an average of 1.0927 m^2/g. The PV values are between 3.84 $\times$ 10^{-3} cm^3/g and 9.09 $\times$ 10^{-3} cm^3/g, with an average of 5.92 $\times$ 10^{-3} cm^3/g, and the d_a varies from 18.99 nm to 32.99 nm, with a mean of 26.74 nm (Table 2). The H2-H3 shale has a relatively high SSA and a relatively low d_a. Types H3 and H2-H3 shales have similar PV, with mean values of 5.77 $\times$ 10^{-3} cm^3/g and 6.12 $\times$ 10^{-3} cm^3/g, respectively.

Table 2. Pore structure parameters of shale from Fengcheng Formation.

Sample	Pore Parameters of Study Samples from N_2 Adsorption			
	BET SSA/ (m^2/g)	Pore Volume 10^{-3} (cm^3/g)	Average Pore Diameter/nm	Loop Type
HSX1-1	0.5971	4.48	32.47	H3
HSX1-2	1.5058	5.80	19.57	H2-H3
HSX1-4	0.6390	3.84	26.78	H3
HSX1-6	1.1829	6.30	24.21	H2-H3
HSX1-7	1.1824	9.09	32.99	H3
HSX1-8	0.7649	5.67	32.16	H3
HSX1-12	1.7765	6.26	18.99	H2-H3

The PV of shale samples is mainly contributed by meso- and macropores. The mesopore PV accounts for 44.15% to 57.17% of the PV, with an average of 50.15%. The macropore PV accounts for 41.65% to 55.05% of the PV (mean 48.84%), while the micropore PV contributes the least, on average, 1.01% (Figure 5). H3 shales have high macropore contents, ranging from 51.53% to 55.05%; conversely, the mesopore content of H2-H3 shale is higher, varying from 41.65% to 46.23%. The SSA of shale is mainly constituted of mesopores, ranging from 73.04% to 82.23%, with a mean of 77.01%. The proportion of micro- and macropores is similar, with mean values of 11.46% and 11.53%, respectively (Figure 5).

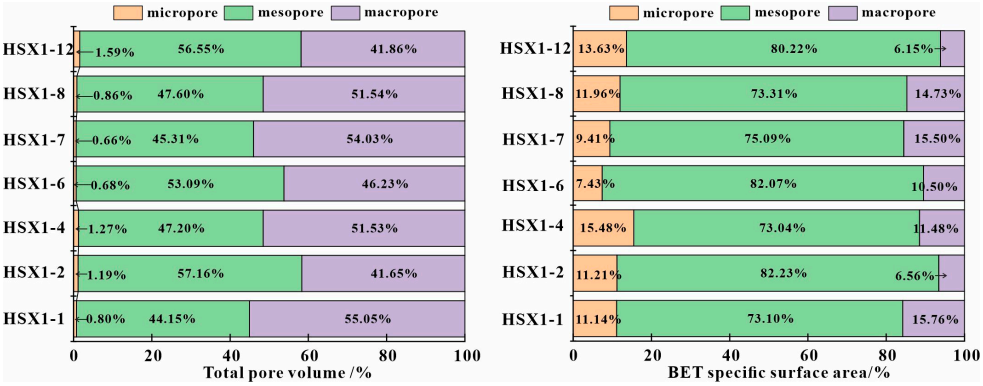

Figure 5. N_2 adsorption total pore volume and BET SSA of shales from Fengcheng Formation.

The N_2 adsorption pore size distribution of shale samples is illustrated in Figure 6. The Type H2-H3 shales exhibit two peaks, the right peak at about 70 nm and the left peak at 3 nm. The Type H3 shales exhibit a single peak at 70 nm. It can be concluded that the content of macropores in Types H3 and H2-H3 shales is very high, while Type H2-H3 shales develop a small number of micro- and mesopores (Figure 6).

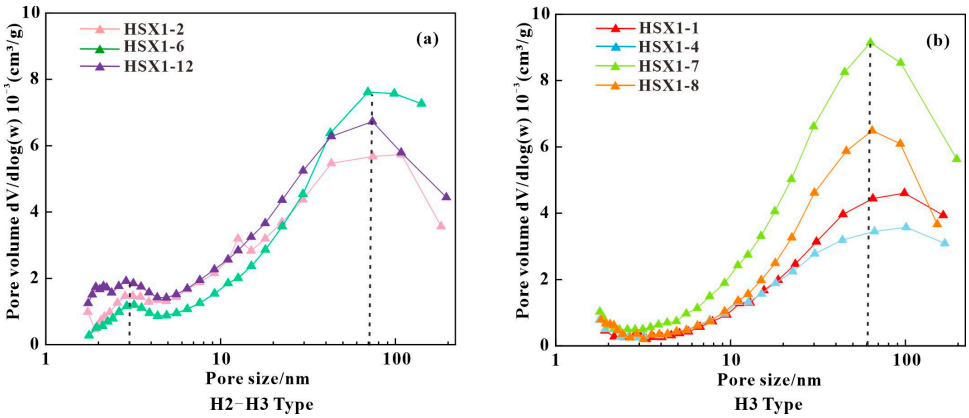

Figure 6. Pore size distributions of the Fengcheng Formation shales from N_2 adsorption: (**a**) The N_2 adsorption pore size distribution of Type H2-H3 shales. (**b**) The N_2 adsorption pore size distribution of Type H3 shales.

4.4. Fractal Characteristics of Microscopic Pore Structure

4.4.1. Single-Fractal Characteristics

N_2 adsorption fractal theory is commonly used to characterize the heterogeneity of shale microscopic pore structure. At a relative pressure (p/p_0) of 0–0.5, the fractal dimension is represented by D_1, reflecting the complexity of the shale pore surface morphology. At a relative pressure (p/p_0) of 0.5–1.0, the fractal dimension is represented by D_2, representing the complexity of the shale pore structure [41] (Figure 7). Where D is between 2 and 3, the surface of the shale sample is rougher and the pore structure is more complex as the fractal dimension D approaches 3; the pore structure of the shale is simpler as D approaches 2 [46,47]. The D_1 of the studied shales ranges from 2.3752 to 2.5371, with an average of 2.4644, and the D_2 varies from 2.3596 to 2.5337, with a mean value of 2.4355 (Table 3). In general, the H3 shale has a lower fractal dimension, D_2, indicating a simpler pore structure.

4.4.2. Multi-Fractal Characteristics

According to the sample HSX1-1, the log–log plot of the partition function x (q, ε) and the length scale ε shows a clear linear correlation (Figure 8a); i (q) exhibits a strictly

monotonically increasing trend; and D_q exhibits a strictly monotonically declining curve with an increase in q (Figure 8b,c). The relationship between a and f (a) in the multifractal spectrum displays an image of a convex function (Figure 8d). All of the above indicates that the shale pore structure has multifractal characteristics.

The D_q spectrum can indicate differences in the internal distribution of shale pore size, and the D_q width $D_{-10}-D_{10}$ depicts pore spatial heterogeneity across the whole pore size range (1–200 nm) [17]. The strength of pore structure heterogeneity depends on the difference between the D_q value and D_q = 1. The larger the difference, the stronger the heterogeneity, and vice versa. According to Table 4, when q < 0, it reflects the pore distribution of small pore size, indicating the pore distribution characteristics of low porosity area. For example, HSX1-4, HSX1-7, and HSX1-8 have low heterogeneity. When q > 0, it reveals the pore distribution characteristics of the medium and high porosity area. And HSX1-1, HSX1-4, HSX1-7, and HSX1-8 have high heterogeneity.

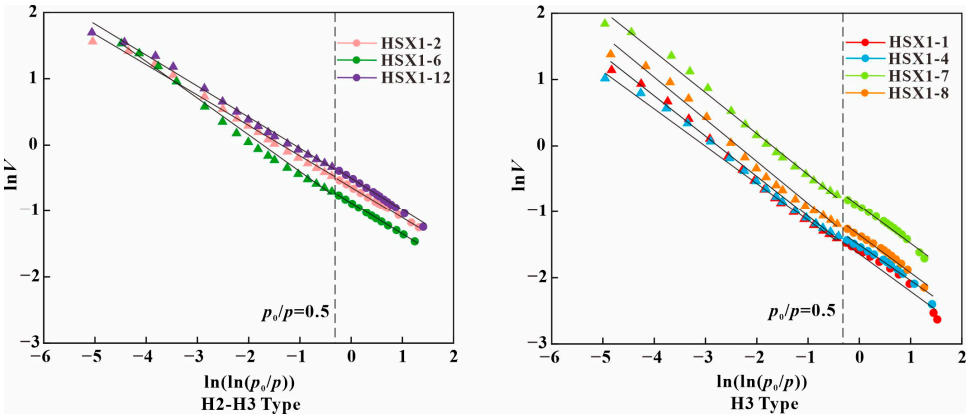

Figure 7. Fractal calculation results from ln (V) vs. ln (ln (p/p_0)) of N_2 adsorption from shales.

Table 3. Fractal dimensions derived from the FHH model.

Sample	$0 < p/p_0 < 0.5$			$0.5 < p/p_0 < 1.0$		
	Fitting Equation	R^2	D_1	Fitting Equation	R^2	D_2
HSX1-1	y = −0.6248x − 1.5672	0.9664	2.3752	y = −0.6238x − 1.7586	0.9945	2.3762
HSX1-2	y = −0.4629x − 0.636	0.9997	2.5371	y = −0.4691x − 0.6545	0.9941	2.5309
HSX1-4	y = −0.5469x − 1.5122	0.9676	2.4531	y = −0.566x − 1.6463	0.9942	2.4340
HSX1-6	y = −0.4731x − 0.8812	0.9995	2.5269	y = −0.5665x − 1.0181	0.9933	2.4335
HSX1-7	y = −0.5576x − 0.9124	0.9810	2.4424	y = −0.6192x − 1.0469	0.9914	2.3808
HSX1-8	y = −0.5605x − 1.3506	0.9759	2.4395	y = −0.6404x − 1.5487	0.9888	2.3596
HSX1-12	y = −0.5232x − 0.4937	0.9990	2.4768	y = −0.4663x − 0.5300	0.9936	2.5337

Table 4. Parameters from fractal dimension spectra of all samples.

Sample	D_0	D_{-10}	D_{10}	$D_{-10}-D_0$	D_0-D_{10}	$D_{-10}-D_{10}$	H	a_{-10}	a_{10}
HSX1-1	1.000	1.626	0.025	0.626	0.975	1.601	0.523	1.848	0.055
HSX1-2	1.000	1.684	0.058	0.684	0.942	1.626	0.552	1.799	0.052
HSX1-4	1.000	1.367	0.039	0.367	0.961	1.328	0.536	1.403	0.035
HSX1-6	1.000	1.650	0.047	0.650	0.953	1.603	0.543	1.765	0.043
HSX1-7	1.000	1.325	0.033	0.325	0.967	1.292	0.529	1.439	0.029
HSX1-8	1.000	1.300	0.034	0.300	0.966	1.266	0.530	1.349	0.030
HSX1-12	1.000	1.728	0.061	0.728	0.939	1.667	0.554	1.848	0.055

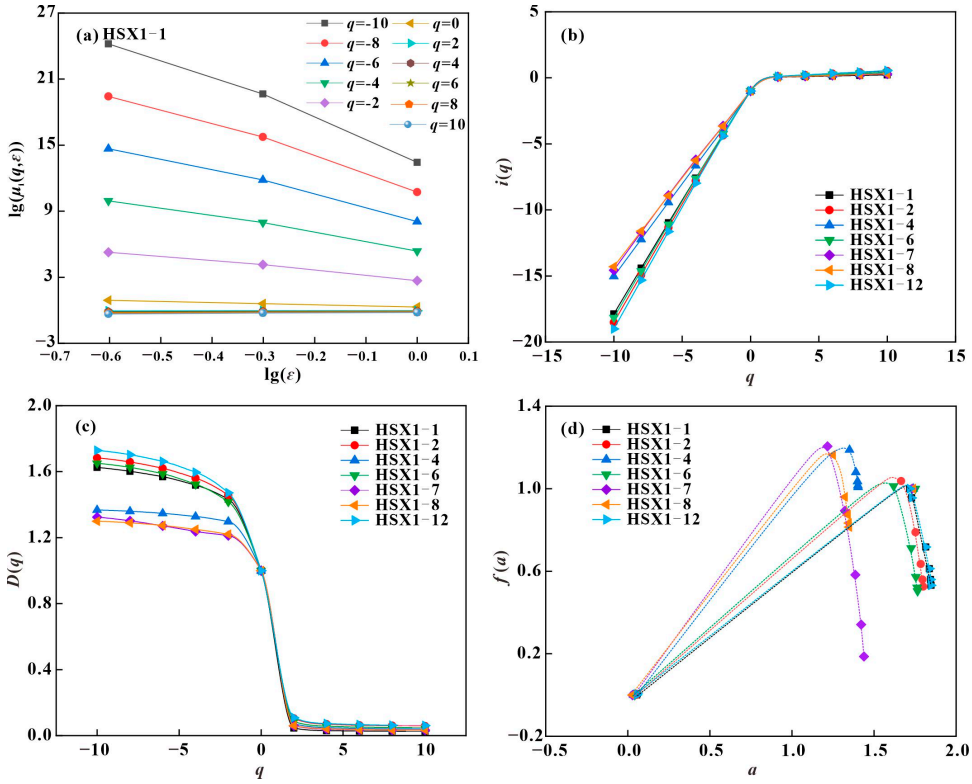

Figure 8. Multifractal analysis of N_2 adsorption: (**a**) The log–log plot of the partition function versus the box scale. (**b**) The relationship between the mass scaling function and the statistical moment order of all samples. (**c**) The generalized fractal dimension spectra of all samples. (**d**) The multifractal singularity spectra of all samples.

The multifractal singular spectrum a~f (a) exhibits a 'U' type distribution with a right hook form, the a_{10} values of shale samples are concentrated, and the a_{-10} values show a right hook shape. It shows that the multifractal spectrum reflects the pore low value information of shale sample.

5. Discussion

5.1. Influencing Factors of Microscopic Pore Structures

According to previous studies, the factors affecting the development of shale reservoir pores are complex and controlled by many factors [48–51]. Sedimentation and tectonic evolution are macro factors affecting pore development, while the mineral composition and OM content are direct factors affecting pore structure [49,52].

The TOC content is negatively correlated with PV and SSA (Figure 9a,b), demonstrating that OM contributes less to the pore volume. The SSA exhibits a weakly positive correlation with plagioclase but a negative correlation with quartz content (Figure 9c). Micro- and mesopore volumes are negatively connected with quartz contents, while macropore volume is the opposite (Figure 9d–f). It demonstrates that macropores are mainly related to quartz, with the peak at about 70 nm in PSDs, because of the stable physical and chemical properties of quartz. Plagioclase and clay mineral contents are weakly positively correlated with micro- and mesopore volumes but weakly negatively related to macropore volume (Figure 9d–f), indicating that micro- and mesopores are primarily associated with plagioclase and clay minerals.

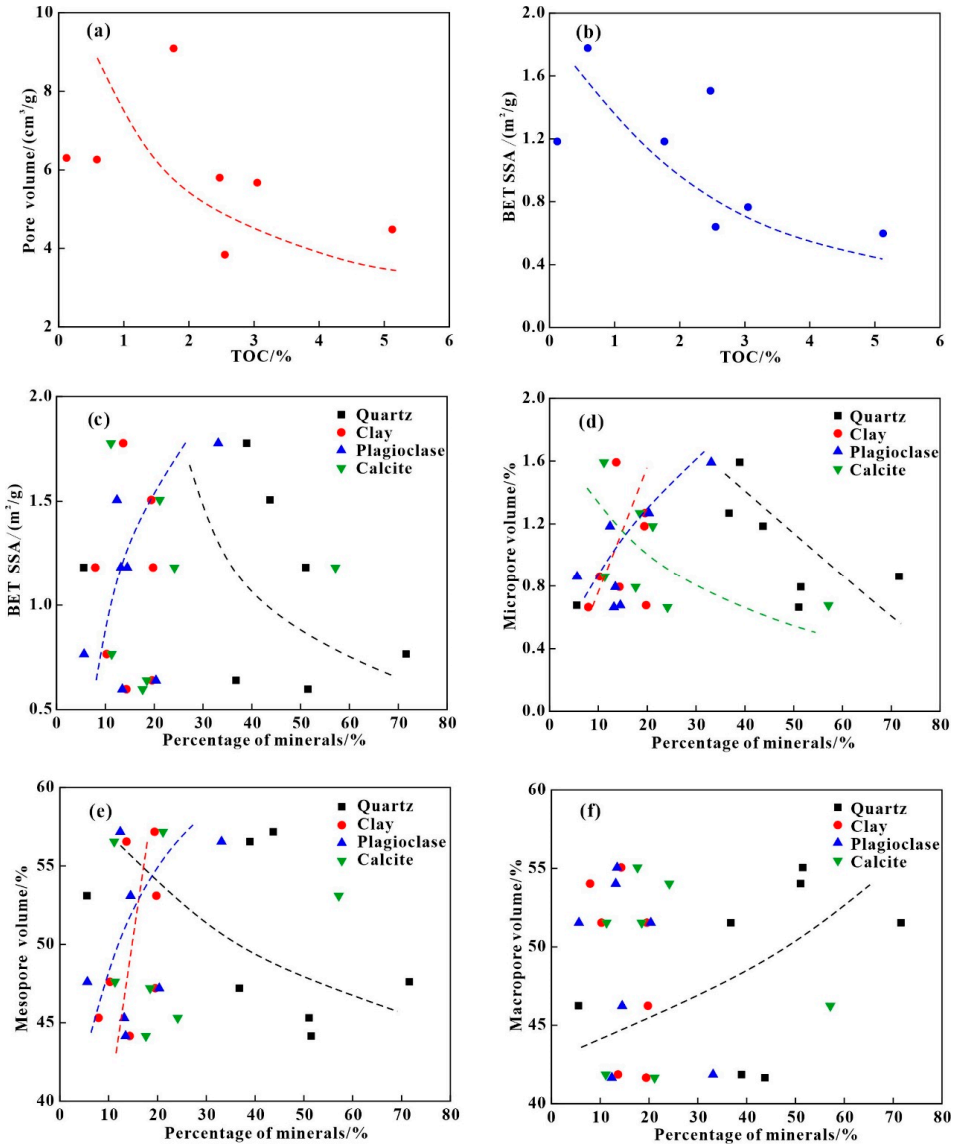

Figure 9. Influencing factors of shale pore structures from Fengcheng Formation: (**a**) Relationship between PV and TOC. (**b**) Relationship between SSA and TOC. (**c**) Relationship between SSA and percentage of minerals. (**d**) Relationship between micropore volume and percentage of minerals. (**e**) Relationship between mesopore volume and percentage of minerals. (**f**) Relationship between macropore volume and percentage of minerals.

5.2. Influencing Factors of Fractal Dimension

5.2.1. Single-Fractal Dimension

The relationships between pore structure parameters and fractal dimension are displayed in Figure 10. A positive correlation between D_2 and SSA indicates that larger SSA leads to a more complex microscopic pore structure of shale. A negative correlation between D_2 and d_a indicates that a larger d_a leads to a simpler microscopic pore structure of shale. Positive correlations between D_2 and micropore PV and mesopore PV values show that large micro- and mesopore PVs correspond to a higher D_2 value and a complex microscopic pore structure. However, macropore PV is negatively correlated with D_2. Therefore, larger SSA and smaller d_a reflect a more complex pore structure or rougher pore surface.

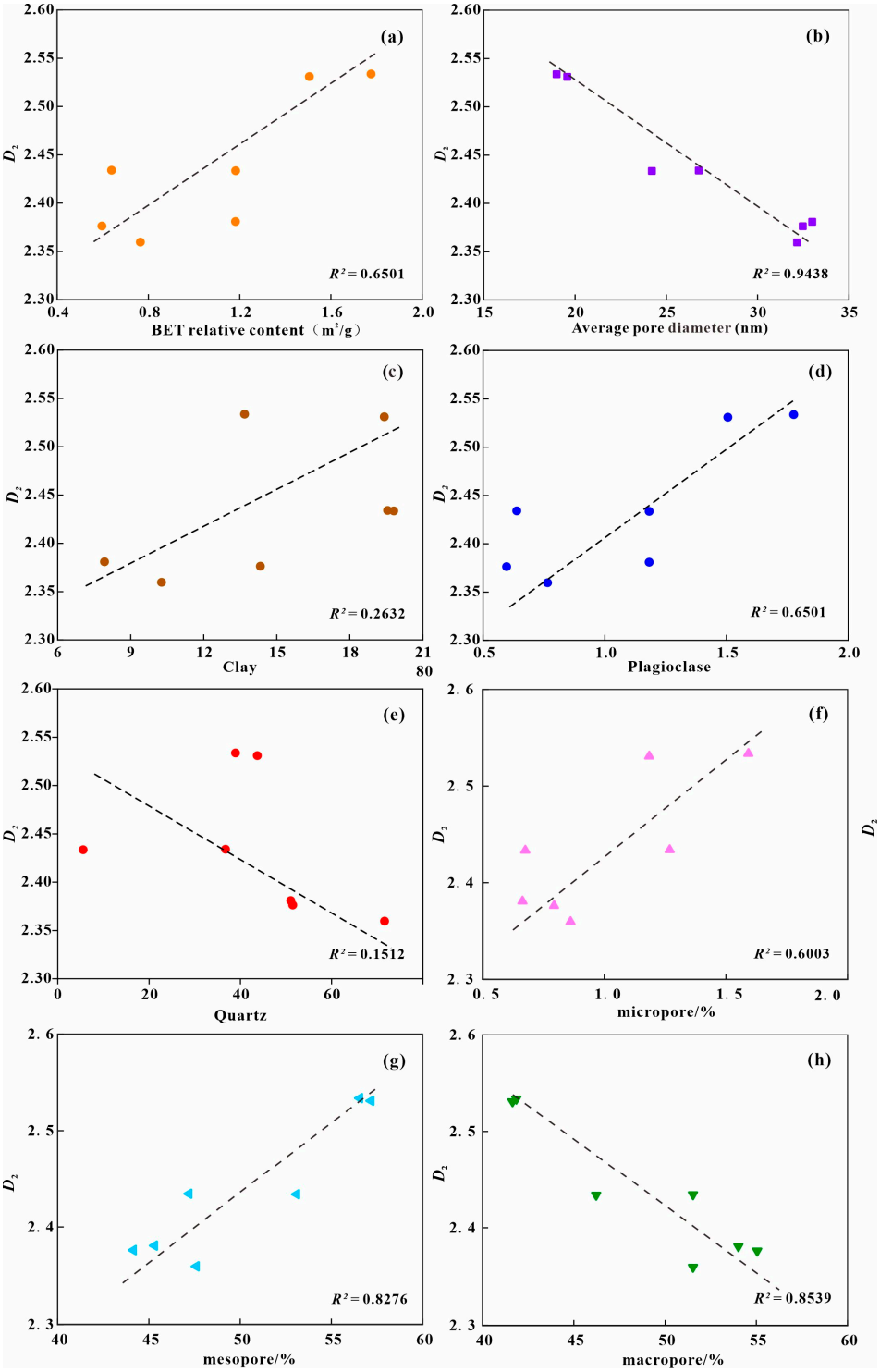

Figure 10. Influencing factors of single-fractal dimension: (**a**) Relationship between D_2 and SSA. (**b**) Relationship between D_2 and d_a. (**c**) Relationship between D_2 and clay content. (**d**) Relationship between D_2 and plagioclase content. (**e**) Relationship between D_2 and quartz content. (**f**) Relationship between D_2 and micropore volume. (**g**) Relationship between D_2 and mesopore volume. (**h**) Relationship between D_2 and macropore volume.

A higher content of quartz implies a higher content of macropores; the higher contents of plagioclase and clay minerals mainly correspond to larger contents of micro- and mesopores. Therefore, both plagioclase and clay minerals have a weak positive affectivity

influence on the heterogeneity of micro- and mesopores (Figure 10c,d,f,g), and quartz has a positive effect on the heterogeneity of macropores (Figure 10e,h).

5.2.2. Multi-Fractal Dimension

The multifractal parameter $D_{-10}-D_0$ mainly represents the difference in the low porosity distribution. Since the pore size distribution of Type H2-H3 shales has a peak at about 3 nm and has a significant $D_{-10}-D_0$ value (Figure 8c), it shows that the enhancement of low porosity heterogeneity of H2-H3 shale is caused by more mesopores.

For the pores parameter of these samples, $D_{-10}-D_0$ has a positive correlation with clay and plagioclase (Figure 11a,b), as well as micro- and mesopore content (Figure 11d,e); both quartz and mesopore contents have positive correlations with D_0-D_{10} (Figure 11c,f). The multifractal properties show that quartz was found to increase pore heterogeneity while plagioclase and clay have an opposite effect.

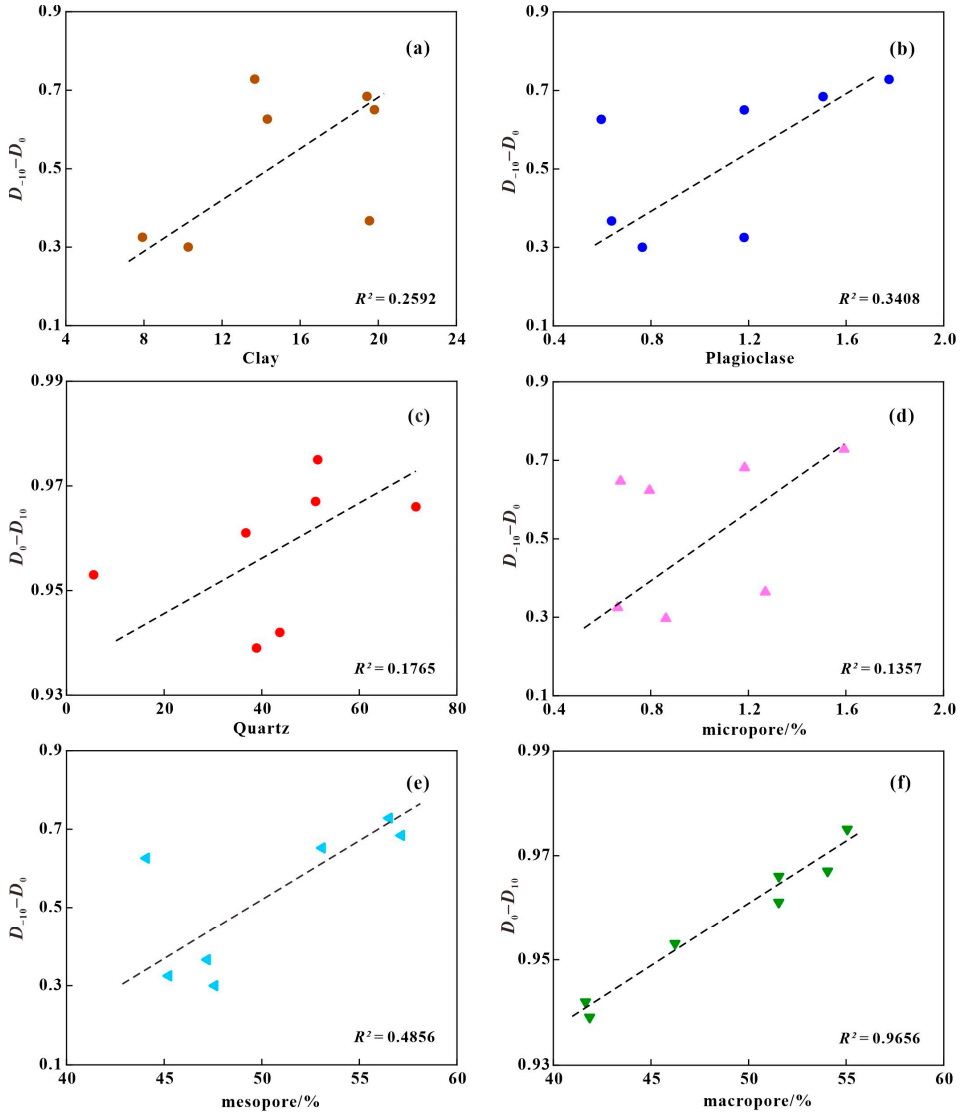

Figure 11. Influencing factors of multi-fractal dimension: (**a**) Relationship between $D_{-10}-D_0$ and clay content. (**b**) Relationship between $D_{-10}-D_0$ and plagioclase content. (**c**) Relationship between D_0-D_{10} and quartz content. (**d**) Relationship between $D_{-10}-D_0$ and micropore volume. (**e**) Relationship between $D_{-10}-D_0$ and mesopore volume. (**f**) Relationship between D_0-D_{10} and macropore volume.

5.2.3. Adaptability Analysis of Fractal Dimension

As correlation analysis is performed on the D_2 and the multifractal parameters $D_{-10}-D_0$, D_0-D_{10}, and $D_{-10}-D_0$, results show that $D_{-10}-D_0$ and $D_{-10}-D_{10}$ exhibit a strong positive correlation and D_0-D_{10} and $D_{-10}-D_{10}$ exhibit a negative correlation (Figure 12a,b). Thus, the pore development in the low-value area plays a leading role in the overall pore heterogeneity of shale. D_2 has a good positive correlation with $D_{-10}-D_0$ and a negative correlation with D_0-D_{10} characterized by a larger correlation coefficient (Figure 12c,d), indicating that D_2 can effectively characterize the heterogeneity of mesoporous pore distribution.

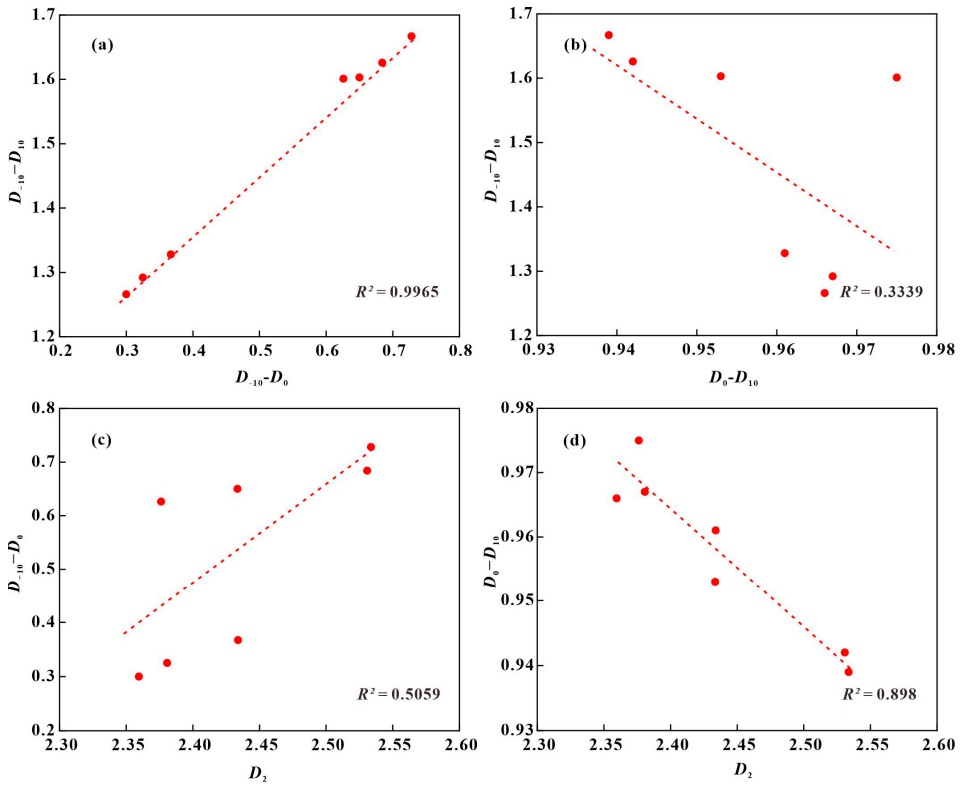

Figure 12. Analysis of single-fractal and multiple-fractal correlation: (**a**) The correlation analysis of $D_{-10}-D_{10}$ versus $D_{-10}-D_0$. (**b**) The correlation analysis of $D_{-10}-D_{10}$ versus D_0-D_{10}. (**c**) The correlation analysis of $D_{-10}-D_0$ versus D_2. (**d**) The correlation analysis of D_0-D_{10} versus D_2.

6. Conclusions

Through a series of experiments and fractal theory, pore structure characteristics and the heterogeneity of the Fengcheng Formation shales were investigated. The following conclusions were drawn:

Two types of pore occurred in the studied area: interparticle pores and intraparticle pores. There were intergranular pores at the edge of quartz and calcite particles, clay mineral intragranular pores were the major pore types and contributed significantly to the reservoir space. The N_2 adsorption curves of shale are characterized as Types H3 and H2-H3. The SSA of Type H2-H3 shales is relatively high, and the d_a is relatively low. Type H3 shale PSDs are unimodal, with a peak at about 70 nm, while Type H2-H3 shales are bimodal, with peaks at about 70 nm and 3 nm, respectively.

The fractal dimensions, D_2, of H3 shales are lower, indicating simpler pore structures. In the multi-fractal spectrum, the $D_{-10}-D_0$ value of H2-H3 shale is higher, which reflects that the heterogeneity of the low-value pore area is higher, and the D_0-D_{10} of H3 shale is higher, indicating that the heterogeneity of the high-value area of H3 shale is higher.

The relationship between pore structure parameters and mineral composition and D_2 shows that the higher the content of micro- and mesopores and the specific surface area, the lower the content of macropores and d_a, and the more complex the microscopic pore structure of shale. The relationship between mineral components and multifractals shows that the effect of plagioclase and clay minerals on the heterogeneity is reflected in the positive effect on micro- and mesopores, and quartz has a positive effect on the heterogeneity of macropores.

The strong correlation between $D_{-10}-D_0$ and $D_{-10}-D_{10}$ suggests that the pore development in the low-value area plays a leading role in the overall pore heterogeneity of shale. Additionally, the correlation between D_2 and D_0-D_{10} is high, indicating that single fractal D_2 can effectively characterize the heterogeneity of mesoporous pore distribution. Therefore, the comprehensive application of single fractals and multifractals can effectively describe the characteristics of shale micropore structure.

Author Contributions: Conceptualization, W.G. and X.C.; methodology, W.G. and P.Z.; validation, W.G., X.C. and P.Z.; formal analysis, Y.W.; investigation, T.G.; resources, Z.Z.; data curation, Z.L.; writing—original draft preparation, W.G.; writing—review and editing, W.G.; visualization, W.G.; supervision, P.Z.; project administration, X.C.; funding acquisition, X.C. All authors have read and agreed to the published version of the manuscript.

Funding: This research was funded by Shandong Province Natural Science Fund for Distinguished Young Scholars (Grant No. JQ201311). And The APC was funded by X.C. (Grant No. 42072172, 41772120).

Institutional Review Board Statement: Not appliable.

Informed Consent Statement: Informed consent was obtained from all sub-jects involved in the study.

Data Availability Statement: Not appliable.

Conflicts of Interest: The authors declare no conflict of interest.

References

1. Zou, C.; Dong, D.; Yang, H.; Wang, Y.; Huang, J.; Wang, S.; Fu, C. Conditions of shale gas accumulation and exploration practice in China. *Nat. Gas Ind.* **2011**, *31*, 26–39.
2. Du, J.; Hu, S.; Pang, Z.; Lin, S.; Hou, L.; Zhu, R. The types, potentials and prospects of continental shale oil in China. *China Pet. Explor.* **2019**, *24*, 560–568.
3. Zou, C.; Yang, Z.; Cui, J.; Zhu, R.; Hou, L.; Tao, S.; Yuan, X.; Wu, S.; Lin, S.; Wang, L.; et al. Formation mechanism, geological characteristics and development strategy of nonmarine shale oil in China. *Pet. Explor. Dev.* **2013**, *40*, 14–26. [CrossRef]
4. Zou, C.; Tao, S.; Hou, L. *Unconventional Petroleum Geology*; Geological Publishing House: Beijing, China, 2011.
5. Boindala, A.; Vij, R.; Avadhani, V.; Pandian, S. Understanding the complexity of thin laminated sequences through reservoir characterization to identify the true potential in Krishna—Godavari offshore area (India): A case study. *Pet. Sci. Technol.* **2022**. [CrossRef]
6. Wang, M.; Xue, H.; Tian, S.; Wilkins Ronald, W.T.; Wang, Z. Fractal characteristics of Upper Cretaceous lacustrine shale from the Songliao Basin, NE China. *Mar. Pet. Geol.* **2015**, *67*, 144–153. [CrossRef]
7. Yang, F.; Ning, Z.; Liu, H. Fractal characteristics of shales from a shale gas reservoir in the Sichuan Basin, China. *Fuel* **2014**, *115*, 378–384. [CrossRef]
8. Wang, P.; Jiang, Z.; Ji, W.; Zhang, C.; Yuan, Y.; Chen, L.; Yin, L. Heterogeneity of intergranular, intraparticle and organic pores in Longmaxi shale in Sichuan Basin, South China: Evidence from SEM digital images and fractal and multifractal geometries. *Mar. Pet. Geol.* **2016**, *72*, 122–138. [CrossRef]
9. Wang, Y.; Pu, J.; Wang, L.; Wang, J.; Jiang, Z.; Song, Y.; Wang, C.; Wang, Y.; Jin, C. Characterization of typical 3D pore networks of Jiulaodong formation shale using nano-transmission X-ray microscopy. *Fuel* **2016**, *170*, 84–91. [CrossRef]
10. Klaver, J.; Desbois, G.; Littke, R.; Urai, J.L. BIB-SEM characterization of pore space morphology and distribution. *Mar. Pet. Geol.* **2015**, *59*, 451–466. [CrossRef]
11. Jiang, B.; Deng, E.; Han, M.; Ma, Z. Microscopic Pore Structure and Fractal Characteristics from Xiangbai Formation Shale of Carboniferous in Northwest Guizhou. *Geoscience* **2022**, *36*, 1065–1073.
12. Jouini, M.S.; Bouchaala, F.; Riahi, M.K.; Sassi, M.; Abderrahmane, H.; Hjouj, F. Multifractal Analysis of Reservoir Rock Samples Using 3D X-Ray Micro Computed Tomography Images. *IEEE Access* **2022**, *10*, 67898–67909. [CrossRef]
13. Zhang, P.; Lu, S.; Li, J.; Chen, C. Petrophysical characterization of oil-bearing shales by low-field nuclear. *Mar. Pet. Geol.* **2018**, *89*, 775–785. [CrossRef]

14. Torre, I.G.; Martín-Sotoca, J.J.; Losada, J.C.; López, P.; Tarquis, A.M. Scaling properties of binary and greyscale images in the context of X-ray soil. *Geoderma* **2020**, *365*, 114205. [CrossRef]
15. Wang, M.; Jiao, C.; Li, C.; Li, Z.; Zhou, N.; Li, J.; Lu, S.; Tian, F.; Hao, G.; Shi, J. Multi-fractal characteristics of micro-pores ofShahejie Formation shale in Dongying Sag. *Pet. Geol. Recovery Effic.* **2019**, *26*, 72–79.
16. Zhang, N.; Xun, X.; Wang, S.; Zhang, H. Calculation of multi-fractal dimension of coal measure sedimentaryrock and analysis of influencing factors. *J. Min. Sci. Technol.* **2021**, *6*, 623–632.
17. Ma, H.; Li, W. Multifractal Characterization of Low-temperature Nitrogen Adsorption for Pore Distribution of Coal. *Saf. Coal Mines* **2020**, *51*, 14–18.
18. Matsushima, J.; Ali, M.Y.; Bouchaala, F. A novel method for separating intrinsic and scattering attenuation for zero-offset vertical seismic profiling data. *Geophys. J. Int.* **2017**, *211*, 1655–1668. [CrossRef]
19. Bouchaala, F.; Ali, M.Y.; Matsushima, J. Compressional and shear wave attenuations from walkway VSP and sonic data in an offshore Abu Dhabi oilfield. *Comptes Rendus. Géosci.* **2021**, *353*, 337–354. [CrossRef]
20. Zhang, P.; Lu, S.; Li, J.; Chang, X.; Li, J.; Li, W.; Chen, G.; Wang, S.; Feng, W. Broad ion beam-scanning electron microscopy pore microstructure and multifractal characterization of shale oil reservoir: A case sample from Dongying Sag, Bohai Bay Basin, China. *Energy Explor. Exploit.* **2020**, *38*, 613–628. [CrossRef]
21. Meng, K. Application of multifractal theory in effectiveness evaluation of complex reservoir. *China Univ. Geosci.* **2021**. [CrossRef]
22. Zhang, P.; Yin, Y.; Lu, S.; Li, J.; Chang, X.; Zhang, J.; Pang, Y.; Chen, G.; Liu, Y.; Li, Z. Insights into Pore Structures and Multifractal Characteristics of Shale Oil Reservoirs: A Case Study from Dongying Sag, Bohai Bay Basin, China. *Energy Fuels* **2022**, *36*, 8224–8237. [CrossRef]
23. Liu, K.; Ostadhassan, M.; Zou, J.; Gentzis, T.; Rezaee, R.; Bubach, B.; Carvajal-Ortiz, H. Multifractal analysis of gas adsorption isotherms for pore structure characterization of the Bakken Shale. *Fuel* **2018**, *219*, 296–311. [CrossRef]
24. Guan, M.; Liu, X.; Jin, Z.; Lai, J. The heterogeneity of pore structure in lacustrine shales: Insights from multifractal analysis using N_2 adsorption and mercury intrusion. *Mar. Pet. Geol.* **2020**, *114*, 104150. [CrossRef]
25. Zhang, S. Identification and its petroleum geologic significance of the Fengcheng Formation source rocks in Hala'alt area, the northern margin of Junggar Basin. *Oil Gas Geol.* **2013**, *34*, 145–152.
26. Zhi, D.; Song, Y.; He, W.; Jia, X.; Zou, Y.; Huang, L. Geological Characteristics, Resource Potential and Exploration Direction of Shale Oil in Middle-Lower Permian, Junggar Basin. *Xinjiang Pet. Geol.* **2019**, *40*, 389–401.
27. Zeng, Z.; Liu, Z.; Zhao, L.; Li, Y.; Wang, C.; Gao, P. Shale oil reservoir characteristics and controlling factors of Permian Fengcheng Formation in Hashan area, northwestern margin of Junggar Basin. *Lithol. Reserv.* **2023**, *35*, 25–35.
28. Song, M. Characteristics and Genetic Analysis for Dolomite Rocks Reservoir of Permian Fengcheng Formation in Hassan Block, the Northern Junggar Basin. *J. Shengli Coll. China Univ. Pet.* **2019**, *33*, 14–18.
29. Li, X.; Zhang, K.; Lin, H.; Zhang, G.; Hou, D.; Wang, S. Sedimentary environment and facies of Permian Fengcheng formation in Hashan and its adjacent areas. *J. Northwest Univ. (Nat. Sci. Ed.)* **2018**, *48*, 699–708.
30. Wang, S.; Wu, Q.; Song, M.; Yu, H.; Zhang, G. Quantitative evaluation of the transportation of fault zone and its controlling effect on hydrocarbon migration and accumulation: Case study of Hala'alat Mountain tectonic belt in the north margin of Junggar Basin. *Nat. Gas Geosci.* **2018**, *29*, 1559–1567.
31. Jia, F. Sedimentary facies and depositional model of Permian Fengcheng Formation in Kexia Area of northwest margin of Junggar Basin. *Fault-Block Oil Gas Field* **2016**, *23*, 681–686.
32. Xue, Y.; Lin, H.; Zhang, K.; Nie, W. Tectonic Characteristics and Genetic Simulation of Hala'alate Mountain Area. *Geotecton. Metallog.* **2017**, *41*, 843–852.
33. Xue, Y.; Zhang, K.; Wang, Y.; Wang, S.; Cheng, S.; Song, M. Techtonic Evolution of Hala'alate Mountain Area and Implications in Petroleum Geology. *Xinjiang Pet. Geol.* **2015**, *36*, 687–692.
34. Sui, F. Tectonic Evolution and Its Relationship with Hydrocarbon Accumulation in the Northwest Margin of Junggar Basin. *Acta Geol. Sin.* **2015**, *89*, 779–793.
35. Yu, H.; Wang, Y.; Zhou, J.; Xue, Y. Sedimentary System of Permian Fengcheng Formation in Hashan Areain Northwestern Margin of Junggar Basin. *Xinjiang Pet. Geol.* **2022**, *43*, 396–403.
36. Xu, L.; Chang, Q.; Feng, L.; Zhang, N.; Liu, H. The reservoir characteristics and control factors of shale oil in Permian Fengcheng Formation of Mahu sag, Junggar Basin. *China Pet. Explor.* **2019**, *24*, 649–660.
37. Pfeifer, P.; Avnir, D. Chemistry in noninteger dimensions between two and three. I. Fractal theory of heterogeneous surfaces. *J. Chem. Phys.* **1983**, *79*, 3369–3558. [CrossRef]
38. Krohn, C.E. Sandstone fractal and Euclidean pore volume distributions. *J. Geophys. Res. Atmos.* **1988**, *93*, 3286–3296. [CrossRef]
39. Yao, Y.; Liu, D.; Tang, D.; Tang, S.; Huang, W. Fractal characterization of adsorption-pores of coals from North China: An investigation on CH_4 adsorption capacity of coals. *Int. J. Coal Geol.* **2008**, *73*, 27–42. [CrossRef]
40. Qi, H.; Ma, J.; Wong, P.-Z. Adsorption isotherms of fractal surfaces. *Colloids Surf. A Physicochem. Eng. Asp.* **2002**, *206*, 401–407. [CrossRef]
41. Wang, X.; Hou, J.; Li, S.; Dou, L.; Song, S.; Kang, Q.; Wang, D. Insight into the nanoscale pore structure of organic-rich shales in the Bakken Formation, USA. *J. Pet. Sci. Eng.* **2020**, *191*, 107182. [CrossRef]
42. Pyun, S.-I.; Rhee, C.-K. An investigation of fractal characteristics of mesoporous carbon electrodes with various porestructures. *Electrochim. Acta* **2004**, *49*, 4171–4180. [CrossRef]

43. Chhabra, A.; Jensen, R.V. Direct Determination of the f(α) Singularity Spectrum. *Phys. Rev. Lett.* **1989**, *62*, 1327–1330. [CrossRef] [PubMed]
44. Thommes, M.; Kaneko, K.; Neimark, A.V.; Olivier, J.P.; Rodriguez-Reinoso, F.; Rouquerol, J.; Sing, K.S.W. Physisorption of gases, with special reference to the evaluation of surface area and pore size distribution (IUPAC Technical Report). *Pure Appl. Chem.* **2015**, *87*, 1051–1069. [CrossRef]
45. Jiang, F.; Huang, R.; Hu, T.; Lv, J.; Huang, L.; Jiang, Z.; Hu, M.; Zhang, C.; Wu, G.; Wu, Y. Geological characteristics and classification evaluation of shale oil in Fengcheng Formation in Mahu sag, Junggar Basin. *Acta Pet. Sin.* **2022**, *43*, 899–911.
46. Xi, Z.; Tang, S.; Li, J.; Li, L. Investigation of pore structure and fractal characteristics of marine-continental transitional shale in the east-central of Qinshui Basin. *Nat. Gas Geosci.* **2017**, *28*, 366–376.
47. Zhang, Y.; Liu, J.; Xu, H.; Niu, X.; Qin, G.; Cao, D. Comparison between pore structure and fractal characteristics of continental and transitional coal measures shale: A case study of Yan' an and Taiyuan formations at the northeastern margin of Ordos Basin. *Acta Pet. Sin.* **2017**, *38*, 1036–1046.
48. Zhao, D.; Guo, Y.; Yang, Y.; Wang, S.; Mao, X.; Li, M. Shale reservoir diagenesis and its impacts on pores of the Lower Silurian Longmaxi Formation in southeastern Chongqing. *J. Palaeogeogr.* **2016**, *18*, 843–856.
49. Gao, Z.; Fan, Y.; Hu, Q.; Jiang, Z.; Huang, Z.; Wang, Q.; Cheng, Y. Differential development characteristics of organic matter pores and their impact on reservoir space of Longmaxi Formation shale from the south Sichuan Basin. *Pet. Sci. Bull.* **2020**, *5*, 1–16.
50. Li, Y. Pore Structure Characteristics of Shale Reservoirs and Their Effects on Oil-bearing Properties in the Zhanhua Sag. *China Univ. Pet.* **2018**. [CrossRef]
51. Xu, J.; Gao, C.; Liu, G. Characteristics and Controlling Factors of Microscopic Pore Structure of Continental Shale Gas in Ordos Basin. *Bull. Sci. Technol.* **2020**, *36*, 17–23.
52. Yang, F.; Meng, X.; Wang, X.; Yu, P.; Shao, G.; Chen, H. Micro-Pore Characteristics and Influencing Factors of Fengcheng Formation Shale in Well Maye-1. *Xinjiang Pet. Geol.* **2022**, *43*, 1–10.